Zi, J.-W., Jourdan, F., Wang. X.-C., Haines, P.W., Rasmussen, B., Halverson, G., Sheppard, S., 2019. Pyroxene 40Ar/39Ar dating of basalt and applications to large igneous provinces and Precambrian stratigraphic correlations. Journal of Geophysical Research, 124, 8313–8330.

# Pyroxene $^{40}Ar/^{39}Ar$ dating of basalt and applications to large igneous provinces and Precambrian stratigraphic correlations

**Jian-Wei Zi[1,2], Fred Jourdan[1,3], Xuan-Ce Wang[3], Peter W. Haines[4], Birger Rasmussen[3], Galen P. Halverson[5], and Stephen Sheppard[3]**

[1] State Key Laboratory of Geological Processes and Mineral Resources, China University of Geosciences, Wuhan, China

[2] John de Laeter Center, Curtin University, Bentley, WA, Australia

[3] School of Earth Science, University of Western Australia, Perth, WA, Australia

[4] Geological Survey of Western Australia, East Perth, WA, Australia

[5] Department of Earth and Planetary Sciences, McGill University, Montréal, QC, Canada

Corresponding author: Jian-Wei Zi (zijw@cug.edu.cn)

**Key Points:**

- We report the first application of pyroxene $^{40}Ar/^{39}Ar$ dating to a Precambrian basaltic lava, the Keene Basalt in central Australia
- The Keene Basalt is correlated with the Mundine Well Dolerite Suite, both being part of a 755-750 Ma LIP related to Rodinia breakup
- The robustly dated Keene Basalt is an important time marker for correlating Neoproterozoic successions in Australia and worldwide

## Abstract

Correlations within and between Precambrian basins are heavily reliant on precise dating of volcanic units (i.e., tuff beds and lava flows) in the absence of biostratigraphy. However, felsic tuffs and lavas are rare or absent in many basins and direct age determinations of Precambrian basaltic lavas have proven to be challenging. In this paper, we report the first successful application of $^{40}Ar/^{39}Ar$ dating to pyroxene from a Neoproterozoic basalt unit, the Keene Basalt in the Officer Basin of central Australia. $^{40}Ar/^{39}Ar$ analyses of igneous pyroxene crystals yielded an age of 752 ± 4 Ma (MSWD = 0.69, probability = 72%), which is underpinned by $^{40}Ar/^{39}Ar$ plagioclase age (753.04 ± 0.84 Ma) from the basalt. This age is significant because the Keene Basalt is one of the very few extrusive igneous rocks identified within the Neoproterozoic successions of central Australia, and is potentially an important time marker for correlating the Neoproterozoic stratigraphy within, and beyond, the central Australian basins. Our geochronological and geochemical data show that the Keene Basalt, which is characterised by enriched elemental and Nd-Pb isotopic signatures, is strikingly similar to, and coeval with, the 755 ± 3 Ma Mundine Well Dolerite Suite in northwestern Australia. Here, we suggest that both are part of the same large igneous province (~6.5 × $10^5$ $km^2$) related to breakup of the supercontinent Rodinia. This study demonstrates the potential of pyroxene $^{40}Ar/^{39}Ar$ geochronology to date ancient flood basalts, and to provide pivotal time-constraints for stratigraphic correlations of Precambrian basins.


## 1. Introduction

Determining the crystallisation age of basaltic lavas is challenging because uranium-rich phases such as zircon are fine-grained and rare in Si-undersaturated volcanic rocks. $^{40}Ar/^{39}Ar$ isotopic dating of mineral separates has been successfully applied to Phanerozoic flood basalts (e.g., Jourdan et al., 2014; Renne et al., 2013), but in Precambrian samples plagioclase, the mineral of choice to date mafic rocks with the $^{40}Ar/^{39}Ar$ technique, is invariably compromised by metamorphic overprinting and/or secondary alteration (Verati & Jourdan, 2014). The occurrence of better preserved K-bearing minerals such as hornblende in mafic rocks is rare, although there are some notable exceptions (Ivanic et al., 2015). However, a recent study by Ware and Jourdan (2018) has shown that pyroxene, an abundant phase in mafic rocks that is resistant to both alteration and mid-temperature metamorphism, can now be precisely dated using a new generation of multi-collector noble gas mass spectrometers. This paper focuses on a basaltic lava, the Keene Basalt, in the Neoproterozoic Officer Basin of central Australia, and represents the first successful application of the new $^{40}Ar/^{39}Ar$ pyroxene approach to a Precambrian basaltic lava.

The Keene Basalt is not exposed at surface but was intersected by GSWA drill-hole Lancer 1, which recovered over 1500 m of continuous core through thick Neoproterozoic sequences in the western Officer Basin in Western Australia. Pisarevsky et al. (2007) carried out systematic paleomagnetic analyses on Lancer 1 drill-core samples, including the Keene Basalt, but the usefulness of the paleomagnetic data are compromised by the lack of robust age constraints. As one of the very rare Neoproterozoic volcanic units in the western Officer Basin, the age and nature of the Keene Basalt is important for several reasons: 1) it can test the relationship between the basalt and known Neoproterozoic igneous events, such as the ca. 825 Ma Willouran–Gardiner large igneous province (Wang et al., 2010; Wingate et al., 1998; Zhao et al., 1994) and the ca. 755 Ma Mundine Well Dolerite Suite (Figure 1) (Li et al., 2006; Wingate & Giddings, 2000); 2) it can be used to calibrate the paleomagnetic data used to reconstruct Australia in Rodina (Pisarevsky et al., 2007), and; 3) it is a possible time marker for Neoproterozoic successions and associated glacial deposits (Halverson et al., 2005; Swanson-Hysell et al., 2012).

The Neoproterozoic evolution of Australia is closely linked to the Rodinia supercontinent (e.g., Pisarevsky et al., 2003). Thick Neoproterozoic successions accumulated in a series of intracratonic basins in central Australia, collectively referred to as the Centralian Superbasin (Walter et al., 1995). The Officer Basin is the largest of these basins and occupies an expansive area across South and Western Australia (Figure 1). Diamond drill-cores recovered from the Officer Basin reveal a depositional history characterised by well-preserved Cryogenian glacial successions (Eyles et al., 2007) formed during the Neoproterozoic snowball Earth intervals (Hoffman et al., 1998). Therefore, the Neoproterozoic stratigraphy in the Centralian Superbasin is important both for reconstructions of Australia in the Rodinia supercontinent cycle (Pisarevsky et al., 2007) and for postulated correlations with Cryogenian glacial successions elsewhere (Eyles et al., 2007).

The timing and tempo of the Neoproterozoic stratigraphy, particularly that associated with the glacial deposits in the Centralian Superbasin has not been well understood, despite significant progress in calibrating Cryogenian glaciations (e.g., Cox et al., 2018; Macdonald et al., 2010; Rooney et al., 2015). It is currently believed that there were two, long-lived global glaciations during the Cryogenian: the Sturtian and the Marinoan. Despite the fact that these informal names are derived from strata in the Adelaide Rift Complex (also known as Adelaide Geosyncline) of South Australia, direct geochronological constraints on Neoproterozoic glacial successions in Australia are rare—a consequence of few available volcanic rocks suitable for geochronology. Assessing the relative stratigraphic positions and correlation of units in the Centralian Superbasin relies on comparing them to, and correlating with, the more continuous successions in the Adelaide Rift Complex (Preiss, 2000) using lithostratigraphy, chemostratigraphy, stromatolite biostratigraphy and palynology (Hill et al., 2011; Walter et al., 1995).

In this context, we carried out an integrated geochronology and geochemistry study to reliably date and genetically characterize the Keene Basalt. Our work demonstrates that the newly developed $^{40}Ar/^{39}Ar$ pyroxene approach, in conjunction with geochemical constraints, can play a crucial role in addressing long-standing, important geological questions.

## 2. Geological Setting and Stratigraphy

### 2.1. The Officer Basin

The Officer Basin straddles Western and South Australia and covers approximately 350,000 km$^2$. It is an intracratonic basin bounded by Precambrian crystalline basement or orogenic belts: to the north by the Musgrave Province, to the southeast by the Gawler Craton, and to the west by the Capricorn Orogen and the Yilgarn Craton (Figure 1). The basin contains thick and well-preserved, but stratigraphically discontinuous Neoproterozoic strata. It is considered to form part of the greater Centralian Superbasin (Walter et al., 1995), which also encompasses the Amadeus, Ngalia and Georgina basins in central Australia (Figure 1), with further connections to Neoproterozoic basins of northern Australia (Haines & Allen, 2017). Each basin has a broadly comparable Neoproterozoic stratigraphy, subdivisible into four depositional supersequences that consist of Tonian siliciclastic, carbonate and evaporitic sediments (Supersequence 1), disconformably overlain by early Cryogenian (Sturtian) glacial sediments and overlying marine shales and carbonates (Supersequence 2), late Cryogenian (early to mid-Marinoan) glacial sediments (Supersequence 3), and Ediacaran siliciclastic sediments (Supersequence 4) (Walter et al., 1995).

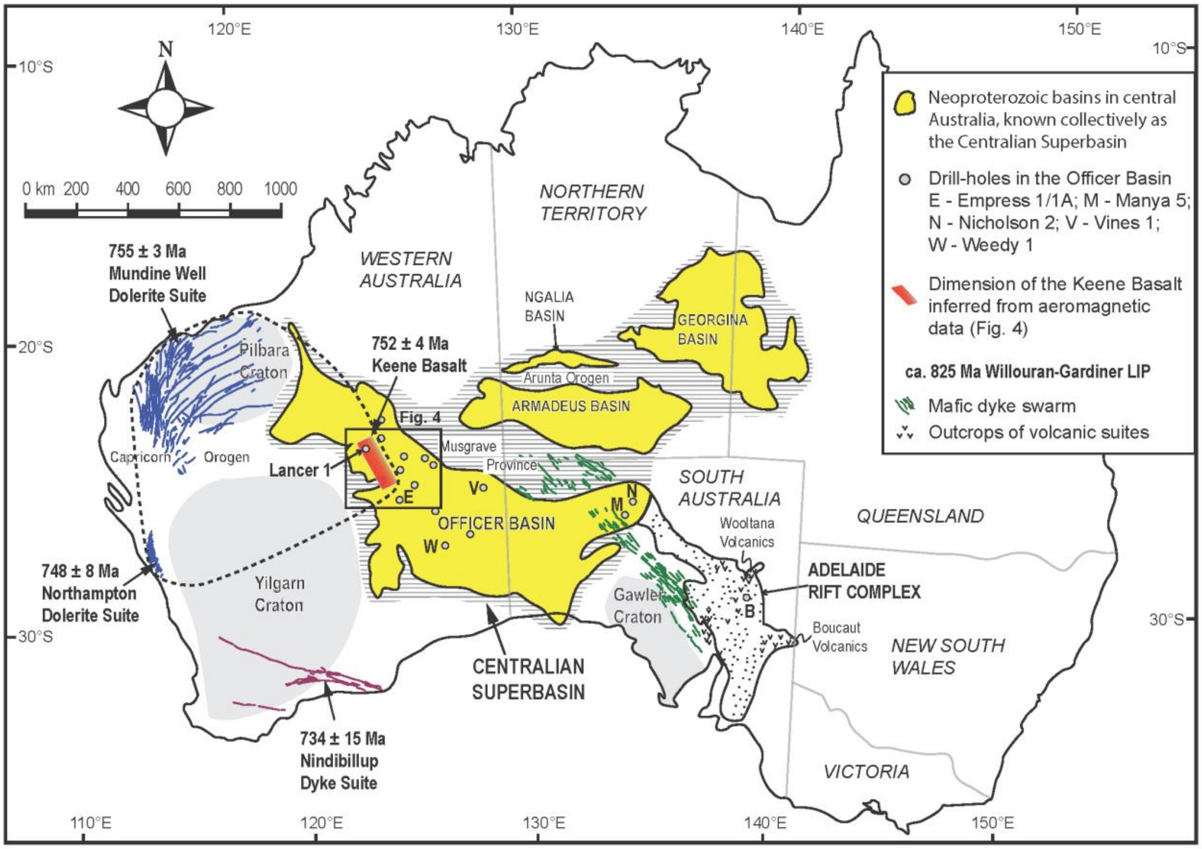


**Figure 1.** Simplified geological map outlining the Centralian Superbasin in central-south Australia and showing location of the GSWA Lancer 1 drill-hole and some other drill-holes in the Officer Basin. Drill-holes relevant to this study are labelled and explained. The age of 755 ± 3 Ma for the Mundine Well Dolerite Suite is based on zircon and baddeleyite U-Pb dating by Wingate and Giddings (2000), and zirconolite U-Pb dating by Rasmussen and Fletcher (2004). The K-Ar age of 748 ± 8 Ma for the Northampton Dolerite Suite is recalculated by Wingate (2017) based on data from Embleton and Schmidt (1985). Note the figure only shows the southern Centralian Superbasin as originally defined by Walter et al. (1995), there is a further connection to the north (Haines & Allen, 2017).

## 2.2. Regional Stratigraphy Revealed by Lancer 1 and Empress 1/1A Drill-holes

Lancer 1, drilled by the Geological Survey of Western Australia (GSWA) in 2003, is located at 25°02′44.5″S, 123°45′20.1″E (GDA94) in the western Officer Basin (Figure 1) (Haines et al., 2004). Lancer 1 was continuously diamond cored from 104 m to a total depth of 1501.3 m, penetrating, in a descending order, the Neoproterozoic Lungkarta, Wahlgu, Kanpa, Hussar and Browne formations of the Officer Basin. The Neoproterozoic rocks are mostly undeformed, resting on Mesoproterozoic and older strata, and overlain by Palaeozoic strata of the Canning and Gunbarrel basins. Based on regional stratigraphy, the Buldya Group, consisting of the Browne, Hussar and Kanpa formations, is assigned to Supersequence 1, the Wahlgu Formation to Supersequence 3, and the Lungkarta Formation to Supersequence 4 (Figure 2). According to Haines et al. (2008), Supersequence 2 is not present in Lancer 1 or Empress 1/1A, but was intersected in the central and eastern parts of the basin (e.g., in drill-holes Vines 1 and Nicholson 2, see Figure 1 for location). The Keene Basalt occurs at ~550 m depth within the Kanpa Formation, in the upper Buldya Group.

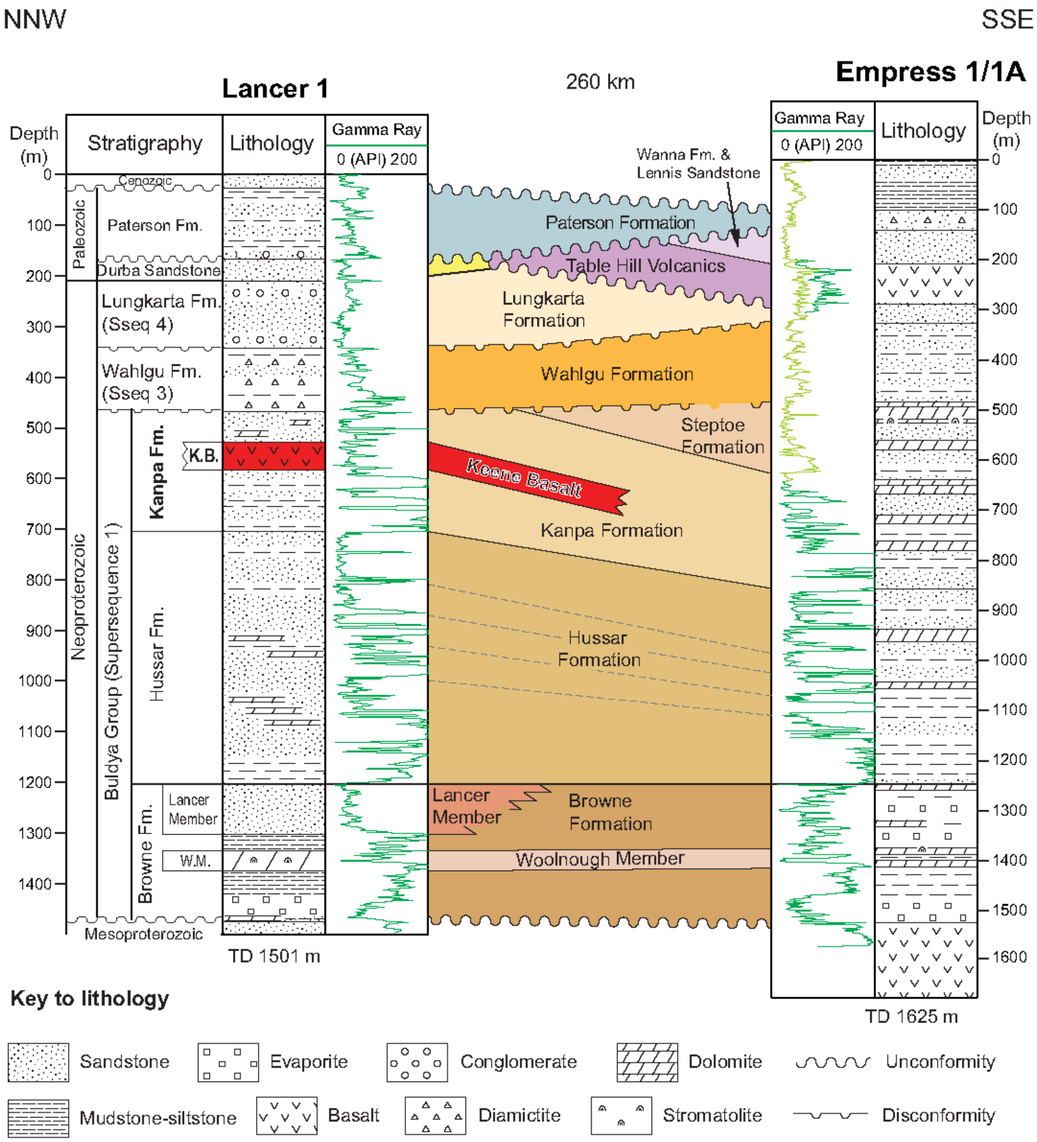


**Figure 2.** Neoproterozoic stratigraphy penetrated by the GSWA drill-holes Lancer 1 and Empress 1/1A (adapted from Grey et al. (2005)). Division of supersequences (SS) follows Walter et al. (1995).

In the Lancer 1 drill-hole, the contact between the Kanpa Formation and the underlying Hussar Formation is a sharp but conformable contact (Figure 2). The Hussar Formation is correlated with the Burra Group in the Adelaide Rift Complex of South Australia (Grey et al., 2005), which is overlain by the Umberatana Group containing the Sturtian and Marinoan glacial units (Figure 3) (Preiss, 2000). The Kanpa Formation contains grey shale beds with carbonaceous disks tentatively identified as megascopic alga *Chuaria sp.*, and possible ash beds (Haines et al., 2004). A sandstone near the top of the Kanpa Formation (between 692.4 and 694.3 m) in Empress 1/1A contains detrital zircons that provide a maximum SHRIMP U-Pb depositional age of 725 ± 11 Ma (2σ) (Grey et al., 2005). A tentative age of 760–720 Ma has been assigned to the Kanpa Formation, based on stromatolite biostratigraphy and palynology, the limited detrital zircon data (Grey et al., 2005), and isotope chemostratigraphic correlation with strata elsewhere (e.g., the ca. 760 Ma Ombombo Supergroup in Namibia, Halverson et al. (2005)). The Kanpa Formation was correlated with the Skillogalee Dolomite and overlying formations in the Burra Group of the Adelaide Rift Complex (Hill & Walter, 2000). However, the Skillogalee Dolomite, at the base of the Burra Group (Figure 3), was recently dated at ca. 790 Ma by zircons from a syn-depositional felsic intrusion and a volcaniclastic siltstone (Preiss et al., 2009). Also near the base of the Burra Group, rhyolites of the Boucaut Volcanics yielded a U-Pb SHRIMP zircon age of 777 ± 7 Ma (Preiss, 2000).

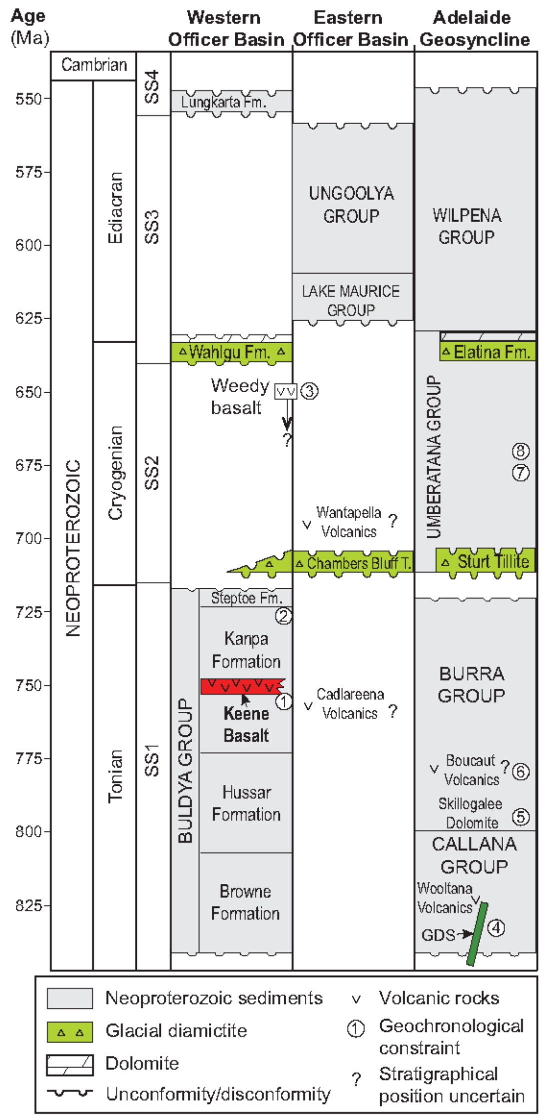


**Figure 3.** Stratigraphical correlation of Neoproterozoic successions in the western Officer Basin with those in the eastern Officer Basin and Adelaide Rift Complex. Simplified stratigraphy of Officer Basin

and Adelaide Rift Complex is based on Grey et al. (2005) and Preiss (2000), respectively. Timescale follows the International Chronostratigraphic Chart v. 2017/02. Source of geochronological data: 1 – Keene Basalt pyroxene, $^{40}Ar/^{39}Ar$ this study; 2 – Kanpa Formation detrital zircon, Nelson (2004); 3 – 'Weedy basalt' K-Ar, Grey et al. (2005); 4 – Gardiner Dyke Swam (GDS) baddeleyite U-Pb, Wingate et al. (1998); 5 – Skillogalee Dolomite zircon U-Pb, Preiss et al. (2009); 6 – Boucaut Volcanics zircon U-Pb, Preiss et al. (2000); 7 – Tindelpina Shale Re-Os, Kendall et al. (2006); 8 – Enorama Shale monazite Th-U-total Pb, Mahan et al. (2010). SS is short for Supersequence.

The Kanpa Formation is overlain by the Wahlgu Formation with an erosional disconformity (Figure 2). The Wahlgu Formation must be younger than ca. 725 Ma (youngest detrital zircon age from upper Kanpa Formation) and older than the ca. 510 Ma Table Hill Volcanics of the Kalkarindji large igneous province (Jourdan et al., 2014), which lie at a higher stratigraphic level in Empress 1/1A (Figure 2). The Wahlgu Formation consists predominantly of glacial diamictite, but the basal part of the unit includes well-sorted sandstone, mudstone and conglomerate. The Wahlgu Formation diamictite is tentatively correlated with the Marinoan glacial succession elsewhere in Australia, e.g., the Elatina Formation in the Adelaide Rift Complex (Figure 3) (Grey et al., 2005; Haines et al., 2004; Walter et al., 1995). The current age constraint for the onset and termination of the Marinoan glaciation is from ca. 640 Ma to ca. 635 Ma (Prave et al., 2016). If the correlation is correct, there is a considerable depositional/erosional hiatus of >80 myr between the Wahlgu Formation and the underlying Kanpa Formation.

### 2.3. Keene Basalt

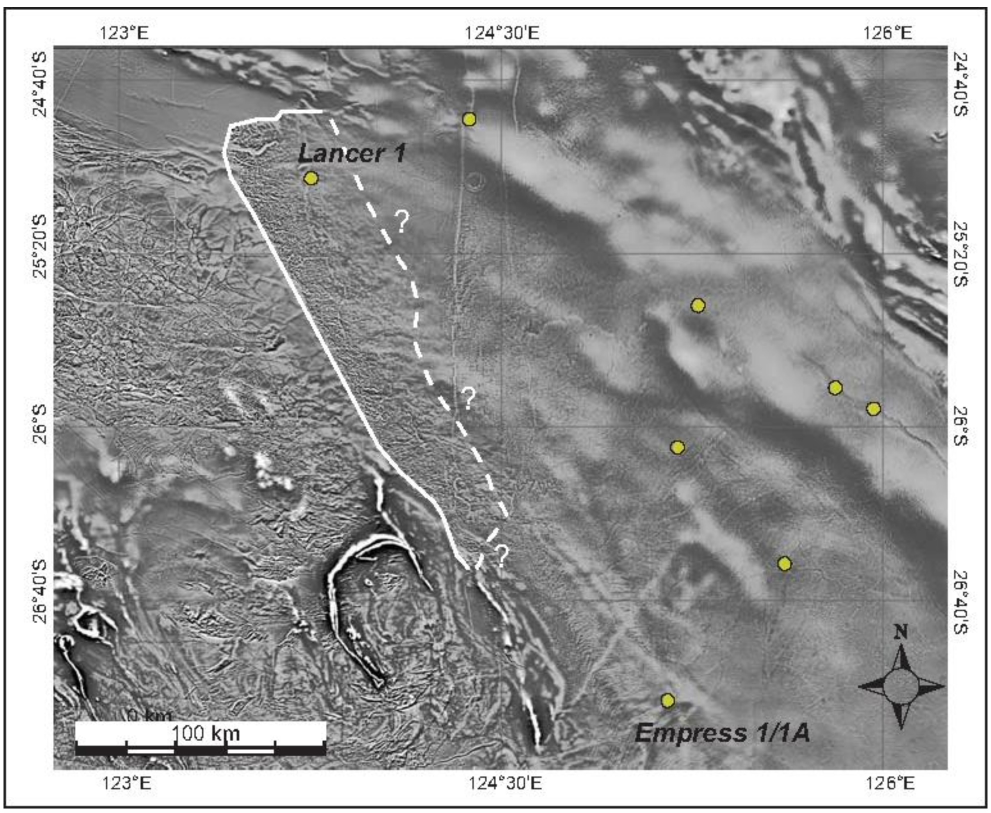


**Figure 4.** Inferred dimension of the Keene Basalt based on aeromagnetic data extracted from the GeoVIEW online database of Geological Survey of Western Australia (June 2017). The western margin

(solid lines) of the basalt is sharp and linear, suggesting fault control, whereas the eastern, southern and northern margins (dashed lines) appear to be more irregular and vague.

The upper Kanpa Formation is interrupted by a suite of basalt flows between 527.4 m and 576.2 m in Lancer 1 (Figure 2). The 48.8 m-thick basalt unit was named the Keene Basalt by Haines et al. (2004), and the drill-hole represents its type section. The basalt unit consists of four or possibly five flows with tops and bases marked by fine-grained amygdaloidal basalt and flow centers of coarse-grained massive basalt (Haines et al., 2004; Pirajno et al., 2006). The top of the uppermost basalt flow lacks the amygdales typical of tops of the underlying basalt, and hence represents an erosional disconformity. It is sharply overlain by ~35 cm of grey, muddy sandstone and stromatolitic dolostone (Haines et al., 2004). The depositional environment before and after basalt extrusion was similar, likely indicating that subsidence kept pace with emplacement of the basalt (Haines et al., 2004).

The Keene Basalt is absent from the Empress 1/1A drill-hole (Figure 2), which is approximately 300 km to the southeast. However, the sub-surface distribution of the basalt unit is interpreted based on aeromagnetic data (Figure 4). The Keene Basalt is elongate in an NNW–SSE direction over a length of >200 km, and its western margin is sharp and linear, suggesting fault control, whereas the eastern, southern and northern margins appear to be more irregular and vague. The possible fault controlling the western margin of the basalt flows appears to be oblique to other faults in the region, but is subparallel to the main structural grain in the Yilgarn Craton (Figure 1). According to Grey et al. (2005), a basalt unit was intersected in drill-hole Weedy 1 located ~550 km SE of Lancer 1 near the southern edge of the Officer Basin (Figure 1). Two samples from the basalt unit (‘Weedy basalt’) yielded K-Ar ages of 657 ± 8 Ma and 640 ± 10 Ma, which were interpreted as the minimum age of the basalt (Grey et al., 2005). It is likely that this basalt unit is a correlative of the Keene Basalt.

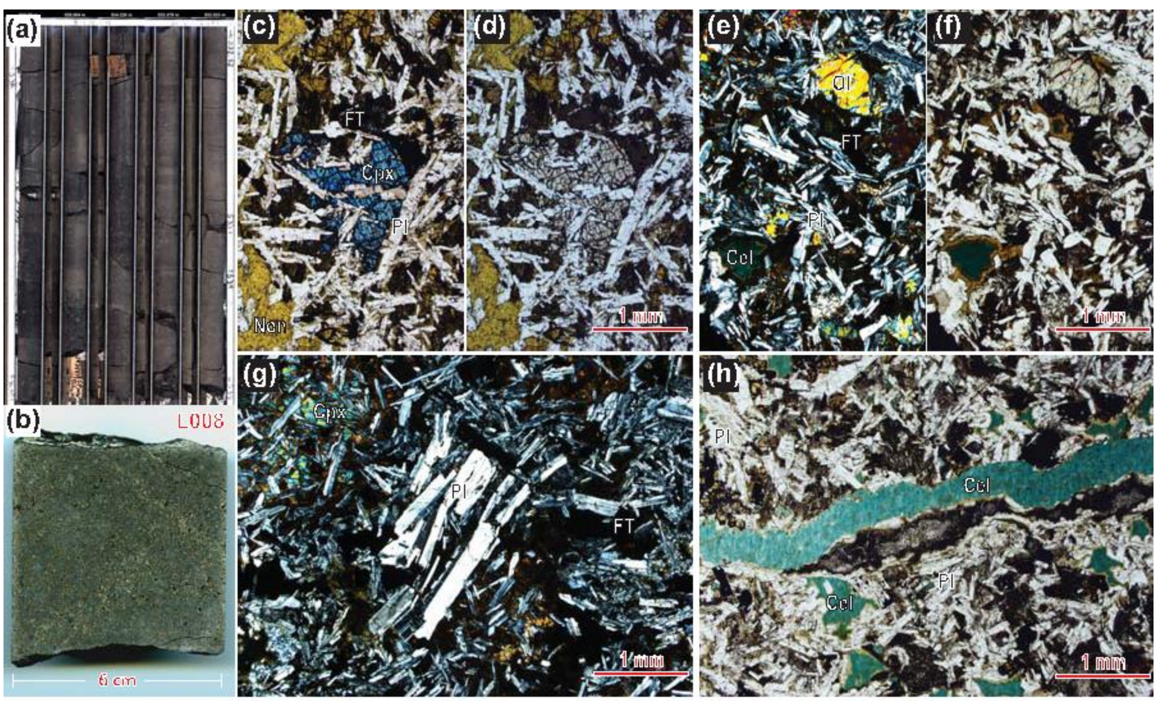


**Figure 5.** (**a**): Photograph of Keene Basalt cores (528.2-532.5 m depth interval) from Lancer 1 drill-hole in the western Officer Basin. Core diameter ~60 mm. (**b**): Photograph of a half-core specimen (sample

L008). (**c**–**h**): Photomicrographs of representative Keene Basalt samples under cross-polarised light (plates c, e and g) and plane-polarised light (plates d, f and h). The basalts are characterised by porphyritic-glomeroporphyritic texture consisting of phenocrysts of olivine (Ol), clinopyroxene (Cpx) and plagioclase (Pl) in a groundmass dominated by plagioclase Fe-Ti oxides (FT) (plates c–g). Celadonite (Cel) fills in cavities or veinlets possibly replacing primary ferromagnesian minerals through hydrothermal alteration, and is commonly lined with clay minerals (plates e, f and h).

The basaltic lavas are typically dark grey to greenish, and fine to medium grained (Figure 5a, b). Vesicular flow bases and tops are characterised by amygdaloidal basalt filled with chlorite, calcite, and red chert. The basalt shows porphyritic or amygdaloidal textures, with phenocrysts consisting mainly of olivine, pyroxene and plagioclase in a groundmass dominated by finer-grained plagioclase, Fe-Ti oxides and sulphides (Figure 5c-g). Primary olivine and pyroxene are replaced by, or partially altered to, celadonite, chlorite and clay mineral nontronite (Figure 5c-d). Plagioclase locally forms glomeroporphyritic aggregates (Figure 5g), whereas celadonite or chlorite are observed to fill pervasive amygdales and/or veins (Figure 5e, f, h).

### 2.4. Neoproterozoic Igneous Events in the Officer Basin and Adjacent Areas

Two major Neoproterozoic igneous events have been documented in the Officer Basin and surrounding areas: namely, the ca. 825 Ma Willouran–Gardiner Large Igneous Province (LIP) and the ca. 755 Ma Mundine Well Dolerite Suite and equivalents (Ernst et al., 2008 and references therein). The Willouran–Gardiner LIP comprises a dense array of mafic dykes and sills and associated volcanic rocks that show broad resemblances in geochemistry and age (Foden et al., 2002; Huang et al., 2015; Wang et al., 2010; Wingate et al., 1998; Zhao et al., 1994). The NW-trending basaltic–doleritic dykes and sills mainly concentrate in a belt starting from the Gawler Craton in the southeast through to the Musgrave Province in the NW, spanning a length of over 1000 km. Outcrops of what are inferred to be associated extrusive suites, including the Wooltana Volcanics and Beda Basalt, are largely confined to the Adelaide Rift Complex (Figure 1).

The Mundine Well Dolerite Suite intruded the Pilbara Craton and the Capricorn Orogen, Western Australia. The dolerite suite has been dated at 755 ± 3 Ma by SHRIMP U-Pb zircon and baddeleyite geochronology from four dykes (Wingate & Giddings, 2000). A similar age (754 ± 5 Ma) has been yielded from the dolerite by Rasmussen and Fletcher (2004) using SHRIMP U-Pb zirconolite. About 450 km to the south, in the Northampton Inlier, a suite of NNE–SSW striking dolerite dykes, referred to as Northampton Dolerite Suite, intruded the Mesoproterozoic metamorphic rocks (Figure 1). The dolerite dykes yielded a K-Ar age of 748 ± 8 Ma (recalculated by Wingate (2017)) with statistically indistinguishable paleopoles to the Mundine Well Dolerite Suite, and hence have been tentatively proposed to be correlative of the latter (Wingate & Giddings, 2000). Further south, on the southeastern margin of the Yilgarn Craton, a mafic dyke of the WNW-trending Nindibillup Dyke Suite (Figure 1) records paleomagnetic directions similar to those for the Mundine Well Dolerite Suite (Pisarevsky et al., 2014), while a dyke of the same suite was recently dated at ca. 734 ± 15 Ma (U-Pb baddeleyite, Wingate (2017)).

## 3. Analytical Methods

### 3.1. $^{40}Ar/^{39}Ar$ Geochronology of Pyroxene and Plagioclase

Samples (L008, L014 and L017) selected for plagioclase and pyroxene separation were first crushed with a steel hydraulic press and then ground by a disk-mill. The material was sieved to a size fraction of 125–212 μm which was washed in distilled $H_2O$ in an ultrasonic cleaner and dried under a heat lamp. Plagioclase and pyroxene were then separated using a Frantz magnetic separator, followed by handpicking under a binocular microscope. Only the most transparent and purest grains were selected. Pyroxene and plagioclase crystals were irradiated for 40 h in one of three irradiation batches at the Oregon State University TRIGA reactor in the Cadmium-Lined In-Core Irradiation Tube (CLICIT) facility. For the first irradiation, plagioclase from sample L014 had a J-value computed as 0.0105574 ± 0.075% (1σ); for the second irradiation, the L008 pyroxene and plagioclase samples had an average J-value of 0.0108832 ± 0.035% (1σ); and for the third irradiation, the L008r pyroxene and L017 plagioclase yielded an average J-value of 0.0106587 ± 0.04% (1σ). Analyses of Ar isotopes of pyroxene and plagioclase were performed using the Western Australian Argon Isotope Facility at John de Laeter Centre, Curtin University using a low volume (600 cc) ARGUS VI multi-collector noble gas mass spectrometer. Fully inter-calibrated standards irradiated together with the samples are GA1550 (age of 99.739 ± 0.100 Ma) and FCs (age of 28.294 ± 0.037 Ma) (Renne et al., 2011). Both the plagioclase and pyroxene crystals were analysed as populations step-heated by a continuous 100 W PhotoMachine© $CO_2$ (IR, 10.4 μm) laser that was fired and rastered onto the sample populations during 60 seconds. The standard analyses were all fused in a single step. The raw data were processed using the ArArCALC software (Koppers, 2002). An extended description of analytical parameters and data processing procedures is given in the Supporting Information (Text S1), and readers are referred to Ware and Jourdan (2018) for further details.

A plateau age is defined as including at least 70% of $^{39}Ar$ released from the analyzed sample, which should be distributed over a minimum of 3 consecutive steps that agree at 95% confidence levels. Furthermore, a probability of fit (P) of ≥ 5% must be satisfied. A plateau age is calculated using the mean of all plateau steps, weighted by the inverse variance of their individual analytical error. Where the accumulative $^{39}Ar$ of calculated steps account for less than 70% (e.g., 60-70%) of released $^{39}Ar$, a mini-plateau age is determined. The (mini-) plateau age is quoted at the 2σ level, which includes analytical J-value errors.

### 3.2. Whole-rock Major and Trace Element Geochemistry

Major and trace element analyses were carried out at the State Key Laboratory of Geological Processes and Mineral Resources, China University of Geosciences, Wuhan. Contents of major oxides were determined using an X-ray fluorescence spectrometer (XRF), following pre-ignition to determine the loss on ignition (LOI) prior to analyses. Analytical precision for major oxide contents was better than 1 percent as estimated from repeat analysis of reference standards. Trace element abundances were determined by Inductively Coupled Plasma-Mass Spectrometry (ICP-MS). Analytical uncertainties were <3% for rare earth elements (REE), <5% for high field strength elements (HFSE) and large ion lithophile elements (LILE) as determined from repeat analysis of AGV-2, BHVO-2, BCR-2, RGM-2.

### 3.3. Whole-rock Nd and Pb Isotopic Compositions

Sm-Nd isotopic data were acquired on a Finnigan Mat 262 thermal ionization mass spectrometer at the Institute of Geology and Geophysics, Chinese Academy of Sciences (IGGCAS). Sample powders were dissolved at low pressure, followed by extraction of Nd using cation exchange and chromatography columns. Procedural blanks were <100 pg for Sm and Nd. $^{143}Nd/^{144}Nd$ was corrected for mass fractionation by normalization to $^{146}Nd/^{144}Nd = 0.7219$. $^{147}Sm/^{144}Nd$ ratios were calculated using the Sm and Nd abundances measured by ICP-MS. Repeated analyses of the BCR-2 and JnDi-1 Nd standards yielded $^{143}Nd/^{144}Nd = 0.512629 \pm 0.000011$ (2σ) and 0.512101 ± 0.000010 (2σ), respectively, in agreement with published reference values.

For Pb isotopic determination, about 100 mg powder was weighted into the Teflon beaker, spiked and dissolved in concentrated HF at 180 °C for 7 h. Pb was separated and purified by conventional cation-exchange technique (AG1 × 8, 200–400 resin) with diluted HBr as an eluant. Total procedure blanks were <50 pg for Pb. Isotopic ratios were measured on a VG-354 Mass Spectrometer at the IGGCAS. Pb reference standard BCR-2 analysed during the analytical session returned isotopic ratios in agreement with established reference values: $^{206}Pb/^{204}Pb = 18.752 \pm 0.002$ (2σ), $^{207}Pb/^{204}Pb = 15.617 \pm 0.002$ (2σ), and $^{208}Pb/^{204}Pb = 38.728 \pm 0.006$ (2σ). External precisions for these ratios are estimated to be better than 0.005, 0.005 and 0.0015, respectively.

# 4 Results

## 4.1. $^{40}Ar/^{39}Ar$ Geochronology

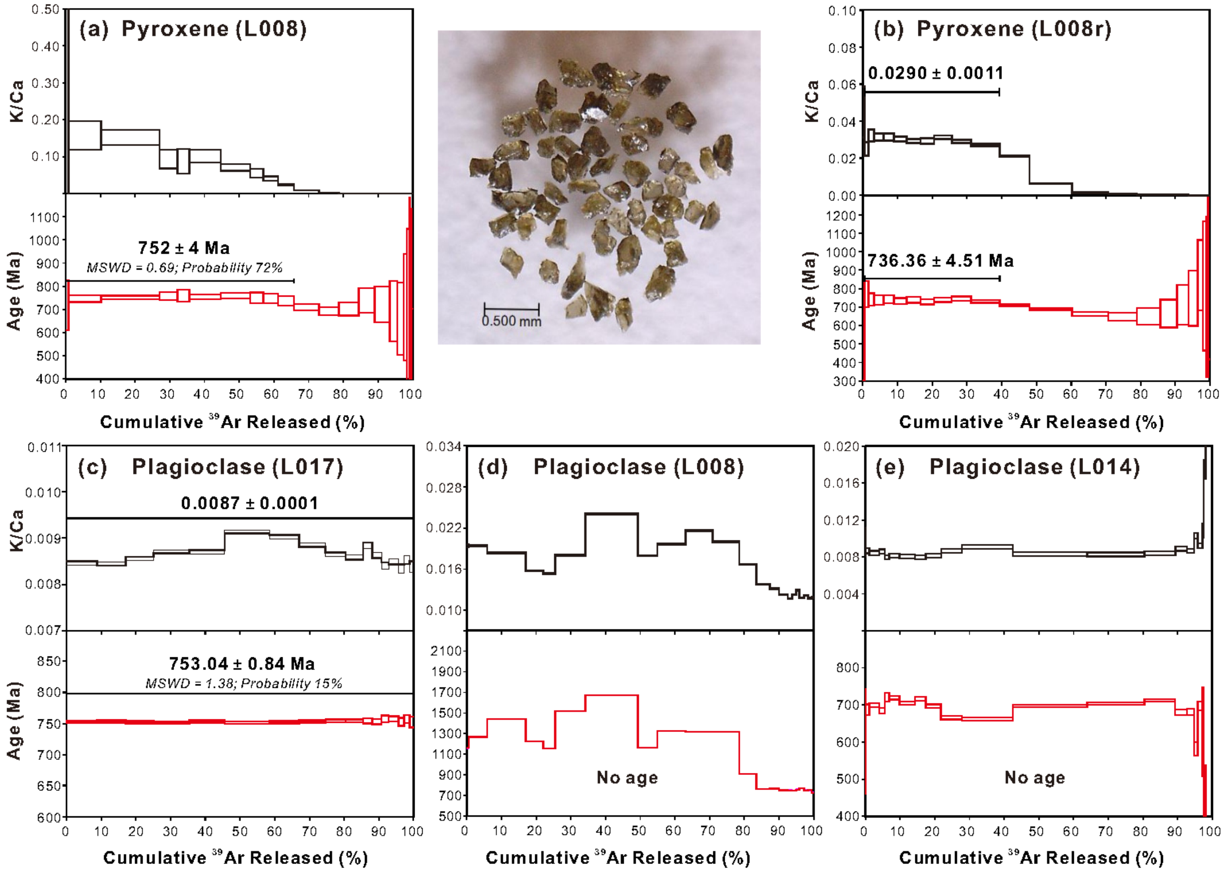


**Figure 6.** Apparent $^{40}Ar/^{39}Ar$ age and K/Ca ratio spectra plotted as functions of fractional release of $^{39}Ar$ for pyroxene (a-b) and plagioclase (c-e) from the Keene Basalt samples. Inset photograph shows pyroxene separates from sample L008 for $^{40}Ar/^{39}Ar$ geochronology. Mean squared weighted deviation (MSWD) and probability of fit are indicated for plateau ages, which are quoted at 2σ uncertainties not including systematic errors (i.e., uncertainties on the age of the monitor and on the decay constant).

Laser step-heating $^{40}Ar/^{39}Ar$ analytical results from Keene Basalt samples are given in the Supporting Information (Tables S1 and S2) and illustrated in Figure 6. Analysis of clinopyroxene from sample L008 yielded a mini-plateau consisting of ten consecutive steps which together account for ~66% of all $^{39}Ar$ released from the sample and define a weighted $^{40}Ar/^{39}Ar$ age of 752 ± 4 Ma with MSWD of 0.69 and probability of 72% (Figure 6a). The inverse isochron age of 756 ± 8 Ma (MSWD = 0.67) agrees with the mini-plateau age, and the $^{40}Ar/^{36}Ar$ intercept value of 297.8 ± 1.5 is statistically identical to the present-day atmospheric value of 298.6 (Mark et al., 2011). A second attempt of analysing pyroxene (L008r) from the same sample did not obtain a statistically robust plateau age, but yielded a semi-quantitative date of 736.36 ± 4.51 Ma (39% released $^{39}Ar$; Figure 6b), interpreted as a minimum age of the sample. In both analyses, the K/Ca ratios of the pyroxene display a similar trend (Figure 6a, b), i.e., largely constant in the range of 0.1-0.2 and 0.02-0.04, respectively, at the low heating steps until about 50% of the $^{39}Ar$

released, after which the ratios steadily decrease and diminish toward the end of the heating processes. This spectrum is analogous to that observed in pyroxene from Phanerozoic dolerites and basalts (Ware & Jourdan, 2018). These authors demonstrated that the high K/Ca ratios shown by the pyroxene samples are readily attributed to the co-existing, clinopyroxene varieties (i.e., high-Ca augite vs. low-Ca pigeonite) being analysed.

Plagioclase grains separated from three samples were analyzed, but only one sample (L017) successfully yielded a plateau age at 753.04 ± 0.84 Ma (MSWD = 1.37, probability = 15%) accounting for 100% released $^{39}Ar$ (Figure 6c). This age closely matches the inverse isochron age of 752.72 ± 1.12 Ma (MSWD = 1.38) for this sample. The K/Ca ratio for plagioclase from sample L017 varies at 0.0087 ± 0.0001 throughout the heating steps with a slight hump in the middle (Figure 6c). Plagioclase separates from the other two samples (L008 and L014) failed to return plateau ages. The apparent $^{40}Ar/^{39}Ar$ age spectrum for plagioclase from sample L008 displays a saddle-like pattern (Figure 6d), which together with its erratic K/Ca suggesting an excess $^{40}Ar$ component (Kelley, 2002), whereas plagioclase from sample L014 yielded a tilde-shape age spectrum (Figure 6e) likely ascribed to the presence of sericite alteration (Verati & Jourdan, 2014). The plateau ages of 752 ± 4 Ma from clinopyroxene and 753.04 ± 0.84 Ma from plagioclase are identical within analytical uncertainties, and the convergence of $^{40}Ar/^{39}Ar$ ages from the two different minerals attests to the robustness of the results.

## 4.2. Geochemistry

Analytical results of major and trace element analyses are given in Supporting Information (Table S3).

The samples show variably high LOI (loss on ignition) ranging from 3.32–8.54 wt% reflecting varying degrees of alteration, which is also evident from the petrographic observations (Figure 5c-h). Analyses with highest LOI (>7 wt%) tend to have lower CaO (0.49–0.66 wt%), $Na_2O$ (0.53–0.72 wt%), Sr (27.5–50.1 ppm) and Ba (48-121 ppm) indicating mobility of these elements during alteration. The elevated $K_2O$ contents for these samples may also be a result of alteration. Total alkalis ($Na_2O$ + $K_2O$) range from 1.77–6.00 wt%, but no correlation between total alkalis content and LOI is observed.

The samples have $SiO_2$ varying from 44.12–51.99 wt% (recalculated volatile-free to 100%; the same calculation was applied to other major oxide contents and ratios presented hereinafter), and MgO from 5.28–13.90 wt% with Mg# (molar Mg/(Mg + Fe)) from 0.41–0.66. The Keene Basalt is characterised by moderate to high $Fe_2O_3$ (11.04–17.12 wt%) and $TiO_2$ (1.88–2.76 wt%) with Ti/Y ratios varying from 365–554. The samples exclusively plot in the field of sub-alkaline basalt on Zr/$TiO_2$ vs. Nb/Y diagram (Figure 7a), and consistently define a tholeiitic trend on the AFM ternary plot (Figure 7b). Chromium and Ni concentrations vary from 51 to 138 ppm and 54 to 114 ppm, respectively.

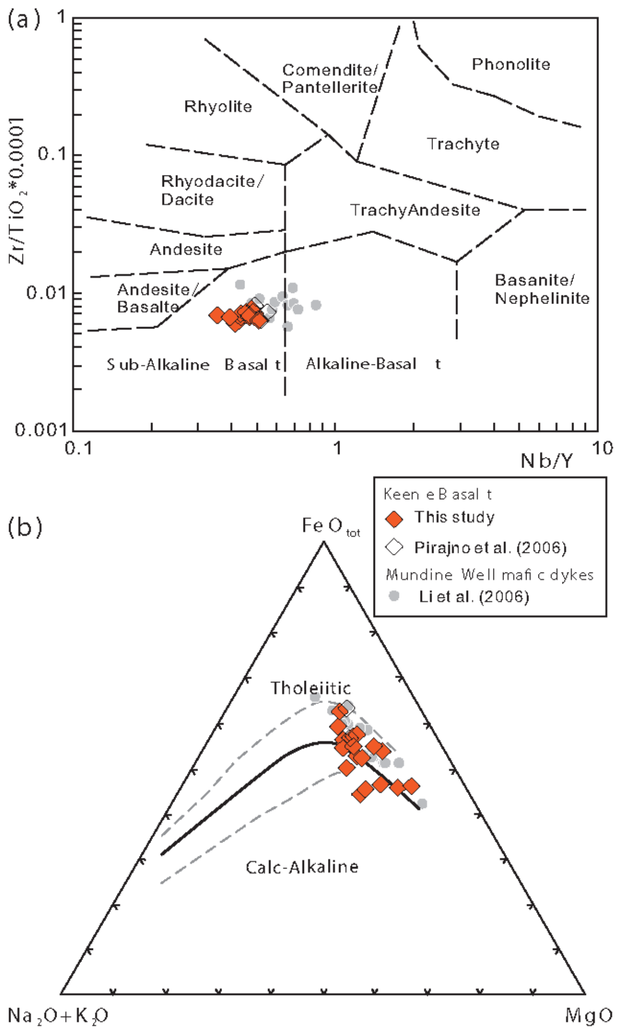


**Figure 7.** (**a**) Zr/$TiO_2$-Nb/Y classification diagram showing that the Keene Basalt samples all fall into the field of Sub-Alkaline Basalt. (**b**) AFM diagram showing a tholeiitic trend defined by the Keene Basalt. Data from the Mundine Well mafic dykes (Li et al., 2006) are plotted for comparison.

The chondrite-normalised REE patterns of these samples show uniform enrichment in the light REEs relative to the heavy REEs with $[La/Yb]_N$ in the range of 4.69–5.75. Most samples display small negative europium anomalies (δEu = 2*Eu/(Sm+Gd); average at 0.89) (Figure 8a). On a primitive-mantle normalised trace element spidergram (Figure 8b), all samples show moderate depletion of Nb and Ta with $[Nb/La]_N$ of 0.53–0.85. The samples that show extreme depletions in Sr ($[Sr/Sr^*]_N$ = 0.07–0.15) correspond to the low-Ca ones characterised by anomalously high LOI values. Except these altered samples, all others have $[Sr/Sr^*]_N$ between 0.53 and 0.70.

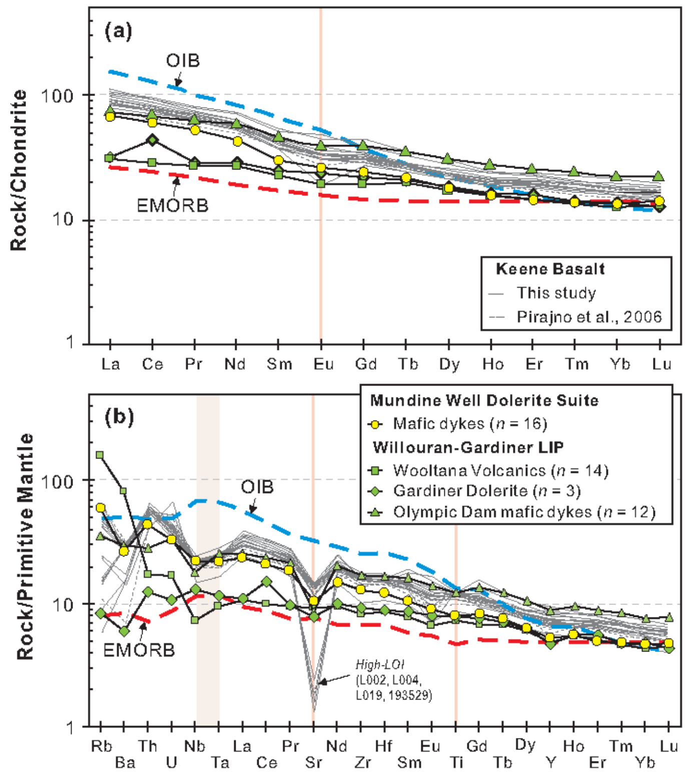


**Figure 8.** (**a**) Chondrite normalised REE patterns and (**b**) primitive-mantle normalised incompatible element spider diagram for samples of the Keene Basalt in comparison with that of the ca. 755 Ma Mundine Well mafic dykes (Li et al., 2006), and the Olympic Dam mafic dykes (Huang et al., 2015) and Wooltana Volcanics (Wang et al., 2010) of the ca. 825 Ma Willouran-Gardiner LIP. Normalisation values are from Sun and McDonough (1989). Note the several high-LOI samples (labelled) show extreme Sr anomalies which may reflect effect of secondary alteration.

Sm-Nd and Pb isotopic data for representative samples of Keene Basalt are given in Supporting Information (Tables S4 and S5). The initial isotopic ratios were calculated using the crystallisation age of the basalts ($t$ = 752 Ma) determined in this study. The analysed basalts show restricted Nd isotopic variations. Overall, the samples show a narrow range of $^{143}Nd/^{144}Nd$ ratios from 0.512341 to 0.512372, and $\varepsilon_{Nd}(t)$ from -0.65 to 0.79 (average 0.09) (Figure 9). In terms of Pb isotopes, with the exception of two samples (i.e., L002 and L004) suspected of severe alteration, the analysed basalts show restricted values of initial $^{207}Pb/^{204}Pb$ (15.65–15.70) and $^{208}Pb/^{204}Pb$ (39.10–39.43) over a small range of $^{206}Pb/^{204}Pb$ (18.29–18.60). The samples are characterised by highly positive Δ7/4 (16.2–21.2) and Δ8/4 (121.8–156.5). In plots of initial $^{207}Pb/^{204}Pb$ and $^{208}Pb/^{204}Pb$ versus $^{206}Pb/^{204}Pb$ (Figure 10), they define Pb isotopic arrays well above the North Hemisphere Reference Line (NHRL; Hart, 1984).

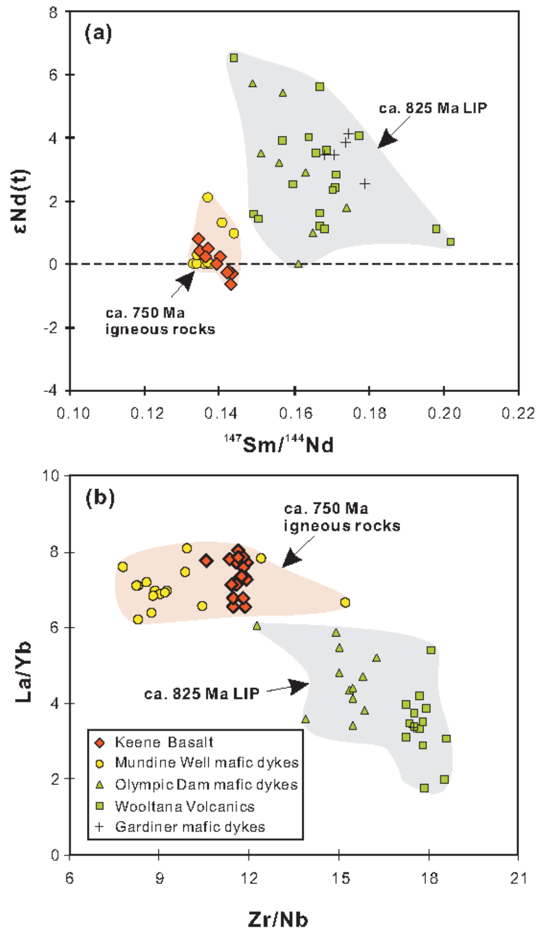


**Figure 9.** (**a**) $\varepsilon_{Nd}$(t) vs $^{147}$Sm/$^{144}$Nd and (**b**) La/Yb vs Zr/Nb diagrams showing the Keene Basalt samples in comparison with known Neoproterozoic mafic rocks in the adjacent areas: the ca. 755 Ma Mundine Well mafic dykes (Li et al., 2006), and intrusive and volcanic units of the ca. 825 Ma Gardiner Large Igneous Province including the Gardiner mafic dykes (Foden et al., 2002; Zhao et al., 1994), the Wooltana Volcanics (Foden et al., 2002; Wang et al., 2010), and the Olympic Dam mafic dykes (Huang et al., 2015).

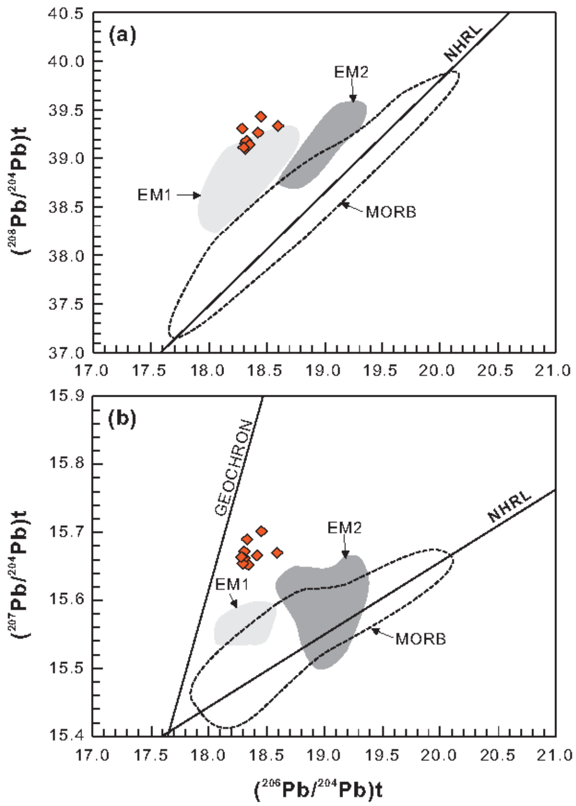


**Figure 10.** Pb isotopic compositions of the Neoproterozoic Keene Basalt (*t* = 752 Ma), compared with approximate fields for MORB, and enriched mantle components EM1 and EM2 (Zindler & Hart, 1986). NHRL, Northern Hemisphere Reference Line (Hart, 1984).

## 5. Discussion

### 5.1. Eruption Age of the Keene Basalt

Clinopyroxene in the Keene Basalt yielded a mini-plateau age of 752 ± 4 Ma (MSWD = 0.69, Probability = 0.72) (Figure 6), although a repeated analysis on the sample produced only a semi-quantitative minimum age of ca. 736 Ma. The latter is likely due to effects of post-magmatic hydrothermal fluid alteration, which might also be responsible for the failure of two out of three attempts in dating the plagioclase from the sample by $^{40}Ar/^{39}Ar$. The third plagioclase sample (L017), however, successfully yielded a plateau age indistinguishable within uncertainty of the pyroxene mini-plateau age, attesting to reliability and robustness of the age. Thus, our $^{40}Ar/^{39}Ar$ results from both pyroxene and plagioclase constrain crystallization age of the Keene Basalt to ca. 753 Ma. This age accords with the correlation of the Hussar Formation with the lower Burra Group (Figure 3), and available radiometric age constraints. Youngest detrital zircons from top Kanpa Formation in Empress 1/1A yielded a SHRIMP U–Pb age of 725 ± 11 Ma (Grey et al., 2005), a maximum depositional age for the host sandstone which lies ~60 m above the basalt horizons (Figures 2 and 3).

The $^{40}Ar/^{39}Ar$ age is indistinguishable within uncertainties from the emplacement ages of the Mundine Well Dolerite Suite (Rasmussen & Fletcher, 2004; Wingate & Giddings, 2000), the Northampton Dolerite Suite (Embleton & Schmidt, 1985; Wingate, 2017), and the Nindibillup

Dyke Suite (Wingate, 2017). The eruption of the Keene Basalt significantly postdates emplacement of the ca. 825 Ma Willouran-Gardiner LIP (Wang et al., 2010; Wingate et al., 1998), and is also ~25 Ma younger than the Boucaut Volcanics (Preiss, 2000), preventing a direct genetic link with those igneous series. Together the new and existing age constraints indicate that the eruption of the Keene Basalt was synchronous with emplacement of the Mundine Well Dolerite Suite (Figure 1) (Li et al., 2006; Wingate & Giddings, 2000).

### 5.2. Petrogenesis of the Keene Basalt

Flows of the Keene Basalt were extruded into a submarine environment and subsequently experienced extensive hydrothermal alteration as indicated by the mineral assemblage present in the samples (Figure 5). Variations in large-ion lithophile elements (LILEs, i.e., K, Rb, Ba and Sr) and high LOI values (3.3–8.5 wt%) (Table 2, Figure 8b) suggest alteration and some degree of mobility. However, the samples show no significant correlations between Rb and Nb, which together with positive correlations between moderately incompatible elements (Zr, La, Th, Ta), imply that the highly incompatible LILEs might have been mobile, whereas the moderately incompatible elements remained immobile during secondary alteration (Wang et al., 2010). Therefore, only Sm-Nd isotopic compositions of least-altered samples (mostly with LOI <4.5 wt%) were determined and considered in discussions of the petrogenesis of the rocks.

Decreased Nb/La and Sm/Nd ratios and low εNd(t) values (and hence positive correlations between them), and Nb-Ta depletions are commonly used as indicators of crustal contamination or assimilation and fractional crystallization (AFC) of mantle derived melts (DePaolo, 1981). Although the Keene Basalt samples show negative Nb-Ta anomalies, their εNd(t) values correlate inversely with Nb/La and Sm/Nd ratios (Figure S1), inconsistent with trends of crustal assimilation or AFC during evolution of the magma.

The samples show variable Mg# values (0.41–0.66) and Ni and Cr concentrations (51–138 ppm and 54–114 ppm, respectively) which are low to moderate when compared with primitive mantle melts (McDonough & Sun, 1995), suggesting that they underwent considerable crystal fractionation during magma evolution. With decreasing Mg#, $SiO_2$ content increases, whereas other major oxides such as $Al_2O_3$ and $Fe_2O_3$t tend to decrease (Figure S2), which may be attributed to the fractionation of olivine and clinopyroxene during early evolution of the magmas, despite no clear covariations being discerned between Mg# and compatible elements Cr and Ni (Figure S2). $TiO_2$ also shows a positive correlation with Mg# (Figure S2), indicating fractionation of Ti-Fe oxides. Although the variable extent of Sr depletion shown by the samples (Figure 8b) can be partly attributed to post-magmatic alteration given mobility of Sr, in conjunction with weak negative Eu anomalies (average δEu of 0.89; Figure 8a), it may also reflect a small degree of fractional crystallisation of plagioclase. The Nb/Ta and Zr/Hf ratios (14.4–18.3 and 34.2–38.0, respectively) of the Keene Basalt are analogous to those of the primitive mantle and typical oceanic basalts (OIBs and MORBs) (Pfander et al., 2007; Sun & McDonough, 1989).

The Keene Basalt displays enrichment of light REEs and highly incompatible trace elements; with the light REE and incompatible trace element abundances mostly falling between the EMORB and OIB. However, the basalt samples show depletions in Nb-Ta and Sr, and their heavy REE abundances are more enriched relative to the OIB and EMORB (Figure 8a,b). The Keene Basalt has slightly enriched Nd isotopic signatures with εNd(t) of -0.65–0.79, and shows elevated $^{208}Pb/^{204}Pb$ and $^{207}Pb/^{204}Pb$ for given $^{206}Pb/^{204}Pb$ (i.e., highly positive Δ8/4 and Δ7/4 values) resulting in conspicuous Dupal anomalies (Hart, 1984) (Figure 10). The enriched Nd-Pb isotopic signatures and presence of negative Nb-Ta anomalies are readily attributed to influence of ancient subduction in the magma source (Baier et al., 2008; Zindler & Hart, 1986). The heavy REE Yb is highly compatible in garnet, compared with the light REEs (e.g., La) and middle REEs (e.g., Sm and Gd), which are incompatible. As a consequence, their ratios e.g., the $[Gd/Yb]_N$ (normalised to chondritic values of Sun and McDonough (1989)) discriminates between garnet- and spinel-dominated source regions. The low to moderate MREE/HREE fractionation ($[Gd/Yb]_N$ = 1.53–2.37, average 1.87) shown by the Keene Basalt suggests that spinel was the predominant phase in the magma source region with melting depth close to the spinel-garnet transition zone (Figure S3).

### 5.3. A Genetic Link with the Mundine Well Dolerite Suite

The two regional-scale Neoproterozoic igneous events across central-west Australia, the ca. 825 Ma Willouran–Gairdner LIP (Wingate et al., 1998; Zhao et al., 1994) and the ca. 755 Ma Mundine Well Dolerite Suite (Figure 1) (Wingate & Giddings, 2000), were succeeded by Cambrian magmatism (the ca. 510 Ma Kalkarinji LIP; Jourdan et al., 2014) represented by the Table Hill Volcanics (intersected in Empress 1/1A drill-hole; Figure 2) in the Officer Basin. The Willouran-Gairdner LIP is predominantly composed of voluminous mafic intrusions, but also incorporates sporadic volcanic rocks—mainly in the Adelaide Rift Complex—that are considered likely extrusive equivalents of the NW-trending dyke swarms that extend over a distance of ~1000 km to the Musgrave Province (Figure 1) (Huang et al., 2015; Wang et al., 2010). However, no well-constrained extrusive rocks coeval with, or equivalent to, the Mundine Well mafic dykes have been identified in Australia.

The $TiO_2$ contents and Ti/Y ratios of the Keene Basalt overlap with those of mafic rocks from both the Willouran–Gardiner LIP (Foden et al., 2002; Huang et al., 2015; Wang et al., 2010; Zhao et al., 1994) and the Mundine Well Dolerite Suite (Li et al., 2006). The Keene Basalt is also akin to the volcanic suites (e.g., the Wooltana Volcanics in the Adelaide Rift Complex) of the Willouran–Gardiner LIP in that both are associated with thick, clastic sedimentary sequences. However, the Keene Basalt is distinctly more enriched in light REEs, characterised by $[La/Yb]_N$ of 4.7–5.8, as compared with the Wooltana Volcanics and Gairdner mafic dykes ($[La/Yb]_N$ = 1.3–4.3, Huang et al. (2015); Wang et al. (2010); Zhao et al. (1994)). Geochemical differences between the Keene Basalt and mafic dykes of the Willouran–Gardiner LIP are also evident in incompatible element ratios such as Zr/Nb (~11.6 vs. ~15.3) and Y/Nb (~2.2 vs. ~4.1). By contrast, the Keene Basalt has many geochemical features in common with the coeval Mundine Well Dolerite Suite. For instance, i) both are characterised by tholeiitic compositions (Figure 7), ii) their REE and incompatible trace element profiles are subparallel to each other but distinct from those of the intrusive and volcanic suites of the Willouran–Gardiner LIP (Figure 8), iii) they have similar $^{147}Sm/^{144}Nd$ ratios and initial εNd values which again are distinct from the Willouran–Gardiner suites (Figure 9); and iv) both show tectonic affinities to within-plate basalts (Figure S4). The striking similarities in age and geochemistry indicate an unambiguous, genetic link between the Keene Basalt and the Mundine Well Dolerite Suite, and corroborate that the former represents the extrusive phase of the igneous event that generated the Mundine Well Dolerite Suite at ca. 755 Ma.

### 5.4. A 755–750 Ma Large Igneous Province Related to Rodinia Breakup

Large igneous provinces are characterised by regional-scale dyke swarms which are generally better preserved than lavas, and in many cases they provide the only record of ancient continental magmatism (Ernst & Buchan, 2003). Evaluation of the original extent and impact of large igneous events is often hampered by poor exposure, particularly the extrusive phases, which are poorly preserved and exposed due to post-magmatic erosion and subsequent burial by widespread younger cover sequences, as is the case for the Keene Basalt in the Officer Basin. The basalt suite appears to be an isolated occurrence, as no surface exposure of the basalt has been recorded, neither has it been identified in any other drill-holes in the Officer Basin. But according to recent aeromagnetic data (Figure 4), the edge of the lava flow is near surface about 20 km west of the Lancer 1 drill-hole and extends south-southeast for about 200 km. It dips gently east-northeast, but the extent remains unconstrained due to depth. However, by recognising the Keene Basalt from drill-core, and establishing its linkage in age and genesis to known dyke swarms, i.e. the Mundine Well Dolerite Suite, we are able to re-evaluate the areal extent of the igneous activity that produced the mafic dykes and basaltic lavas at 755–750 Ma.

The Mundine Well Dolerite Suite is concentrated in the Gascoyne Province of the Capricorn Orogen and extends northeast into the Pilbara Craton. We note that it is possible that the Northampton Dolerite Suite outboard of the northwestern Yilgarn Craton is an equivalent of the Mundine Well dykes based on available K-Ar age and paleomagnetic constraints (Embleton & Schmidt, 1985; Wingate & Giddings, 2000), but intrusions of similar age have not been identified in the interior of the Yilgarn Craton. However, a dyke of the Nindibillup Dyke Suite on the southeastern margin of the Yilgarn Craton yielded paleomagnetic directions consistent with those of the Mundine Well Dolerite Suite and a U-Pb age of 734 ± 15 Ma overlapping with the $^{40}Ar/^{39}Ar$ pyroxene age of the Keene Basalt, thus suggesting that they were possibly emplaced during the same igneous event (Pisarevsky et al., 2014; Wingate, 2017). The magnitude of the igneous event is difficult to determine due to extensive erosion which might have removed much of the lava flows and higher parts of the intrusions. However, taking the Mundine Well Dolerite Suite, Northampton Dolertie Suite and Keene Basalt as extremes, the minimal area affected by the 755–750 Ma igneous event is estimated at ~650,000 km$^2$ across northwestern Australia (Figure 1). If the Nindibillup Dyke Suite proves to be co-genetic, the area affected by the magmatism is nearly doubled in size, entirely covering the two Archean cratons (i.e., the Pilbara and Yilgarn) of Western Australia.

Paleomagnetic analysis of Keene Basalt samples indicates low to moderate paleolatitudes (mean = 17.6°) (Pisarevsky et al., 2007), consistent with reconstruction models of supercontinent Rodinia in which Australia constitutes a core component situated near the equator at ca. 750 Ma (Pisarevsky et al., 2003). Neoproterozoic magmatism of similar age (ca. 750 Ma) is recorded in many other continental blocks constituting Rodinia, such as South China, India, Seychelles, Madagascar and southern Africa (Ernst et al., 2008 and references therein). Genesis of the widespread mafic magmatism at ca. 750 Ma has been related to decompressional melting of mantle in a passive rift setting, or to large-scale lithosphere-asthenosphere interactions possibly caused by plume activity (e.g., Li et al., 2006; Torsvik et al., 2001) during breakup of the Rodinia supercontinent (Ernst et al., 2008; Pisarevsky et al., 2003; Wingate & Giddings, 2000).

### 5.5. A New Time Marker for Correlating Stratigraphy Associated with Cryogenian Glacial Successions

Although the Keene Basalt seems to comprise a series of flows restricted to the western part of the Officer Basin, core logging and petrographic observations demonstrate that the top of the basalt unit was uplifted and the flow top truncated by erosion before sedimentation resumed (Haines et al., 2004). The 'Weedy basalt' is likely equivalent to the Keene Basalt, based on its stratigraphic positions and interpretation of its K-Ar age of ca. 650 Ma as a minimum age (Grey et al., 2005). Another possible equivalent of the Keene Basalt is the Cadlareena Volcanics in the eastern Officer Basin (Figures 1 and 3), which are 79 m thick in the Manya 5 drill-hole (Figure 1) and >700 m in outcrop (Morton, 1997). These volcanic rocks are unconformably overlain by Cryogenian glacial successions (i.e., the Chambers Bluff Tillite) and the unit has been tentatively correlated with the ca. 777 Ma Boucaut Volcanics in the Adelaide Rift Complex (Hill et al., 2011; Morton, 1997). However, the Cadlareena Volcanics also occurs near the top of the global Bitter Springs negative carbon isotope anomaly (Swanson-Hysell et al., 2010), which occurs throughout the Centralian Superbasin, including within the middle Hussar Formation in the western Officer Basin (Hill & Walter, 2000). The end of Bitter Springs anomaly is constrained to be > ca. 789 Ma based on U-Pb zircon ages from the Tambien Group of Ethiopia (Swanson-Hysell et al., 2015). If the Cadlareena Volcanics are equivalent to the Keene Basalt, the implication is that the contact below them (with the Coominaree Formation) is an unconformity representing >35 m.y. of non-deposition and erosion. Alternatively, the Cadlareena Volcanics represent an older magmatic episode with no known expression in the western Officer Basin.

Isotope chemostratigraphy, in particular the application of carbon isotope ($\delta^{13}C$) data, has been used to correlate the Kanpa Formation with pre-Cryogenian successions in the Adelaide Rift Complex (the upper Burra Group) and their purported equivalents in Canada, Spitsbergen, and Namibia (Hill & Walter, 2000; Walter et al., 2000). The new radiometric age from the Keene Basalt sandwiched in the Kanpa Formation provides a geochronological constraint on such stratigraphical correlations and a potential calibration point in the Tonian $\delta^{13}C$ record (Swanson-Hysell et al., 2010). The Kanpa Formation in Empress 1/1A shows a positive excursion in the carbon isotope composition of carbonates, with $\delta^{13}C$ culminated at ~8‰ (Hill & Walter, 2000). These values approximate the heaviest known $\delta^{13}C$ values during Neoproterozoic time prior to the Cryogenian (Halverson et al., 2005; Swanson-Hysell et al., 2010), and similarly $^{13}C$-enriched values occur in the upper Burra Group of the Adelaide Rift Complex and in the middle Ombombo Subgroup of Namibia.

## 6. Conclusions

The application of $^{40}Ar/^{39}Ar$ dating to terrestrial pyroxene enabled us to precisely constrain the eruption age of the Keene Basalt, a series of basaltic lava flows within the Kanpa Formation, which is part of a thick Neoproterozoic sedimentary succession underlying the Cryogenian glacial deposits in the Officer Basin, central Australia. $^{40}Ar/^{39}Ar$ pyroxene and plagioclase geochronology, geochemical data and petrogenetic characterisations collectively demonstrate that the Keene Basalt is coeval and genetically correlated with the Mundine Well Dolerite Suite exposed in northwestern Australia and is significantly younger than the intrusive and volcanic suites of the ca. 825 Ma Willouran–Gardiner LIP. The Keene Basalt, in conjunction with the Mundine Well Dolerite Suite (and perhaps the Northampton Dyke Suite and Nindibillup dolerite suite), suggests the existence of a 755–750 Ma large igneous province emplaced into the crust of western Australia. Basaltic lava flows and dolerite dykes of this age, and with similar compositional characteristics, are globally widespread, and have been collectively related to intraplate rifting or plume magmatism during breakup of supercontinent Rodinia.

Although the dimensions of the Keene Basalt and the regional distribution of its equivalents remain to be accurately determined, it provides a rare and potentially valuable time marker for stratigraphic correlations of Neoproterozoic sedimentary successions including the glacial deposits in the Centralian Superbasin with those in the Adelaide Rift Complex and other continents. The new age constraint from the Keene Basalt supports the correlation of much of the Buldya Group in the western Officer Basin with the Burra Group in the Adelaide Rift Complex and is consistent with available age constraints on the timing of onset of the Cryogenian glaciations (e.g., Macdonald et al., 2010; Rooney et al., 2015). $^{40}Ar/^{39}Ar$ dating of pyroxene from basaltic lavas potentially has an important role to play in dating critical volcanic units in the Neoproterozoic stratigraphy in Australia and worldwide: e.g., in the eastern Officer Basin, the Cadlareena and Wantapella Volcanics that respectively, underlie and overlie the Sturtian-aged glacial succession (i.e., Chambers Bluff Tillite).

## Acknowledgments, Samples, and Data

JWZ and BR acknowledge support from the State Key Lab of Geological Processes and Mineral Resources (MSFGPMR19, GPMR201802), and XCW acknowledges support from the Fundamental Research Funds for the Central Universities (310827163412). We thank the staff of the GSWA Core Library in Perth for providing professional assistance during drill-core inspection and sampling. We acknowledge C. Mayers, A. Frew and Z. Martelli for assistance with the $^{40}Ar/^{39}Ar$ pyroxene and plagioclase sample preparation, X. Qian for help with elemental analyses, and C. Li for assistance with Nd and Pb isotope analyses. PWH publishes with the permission of the Excecutive Director of the Geological Survey of Western Australia. All methods and datasets used in the paper are included as Supporting Information.

## References

Baier, J., Audétat, A., & Keppler, H. (2008). The origin of the negative niobium tantalum anomaly in subduction zone magmas. *Earth and Planetary Science Letters, 267*(1), 290-300. doi:http://dx.doi.org/10.1016/j.epsl.2007.11.032

Cox, G. M., Isakson, V., Hoffman, P. F., Gernon, T. M., Schmitz, M. D., Shahin, S., Collins, A. S., Preiss, W., Blades, M. L., Mitchell, R. N., & Nordsvan, A. (2018). South Australian U-Pb zircon (CA-ID-TIMS) age supports globally synchronous Sturtian deglaciation. *Precambrian Research, 315*, 257-263. doi:https://doi.org/10.1016/j.precamres.2018.07.007

DePaolo, D. J. (1981). Trace element and isotopic effects of combined wallrock assimilation and fractional crystallization. *Earth and Planetary Science Letters, 53*(2), 189-202.

Embleton, B. J. J., & Schmidt, P. W. (1985). Age and significance of magnetizations in dolerite dykes from the Northampton Block, Western Australia. *Australian Journal of Earth Sciences, 32*(3), 279-286. doi:10.1080/08120098508729330

Ernst, R. E., & Buchan, K. L. (2003). Recognizing Mantle Plumes in the Geological Record. *Annual Review of Earth and Planetary Sciences, 31*(1), 469-523.

Ernst, R. E., Wingate, M. T. D., Buchan, K. L., & Li, Z. X. (2008). Global record of 1600–700 Ma Large Igneous Provinces (LIPs): Implications for the reconstruction of the proposed Nuna (Columbia) and Rodinia supercontinents. *Precambrian Research, 160*(1–2), 159-178. doi:https://doi.org/10.1016/j.precamres.2007.04.019

Eyles, C. H., Eyles, N., & Grey, K. (2007). Palaeoclimate implications from deep drilling of Neoproterozoic strata in the Officer Basin and Adelaide Rift Complex of Australia; a marine record of wet-based glaciers. *Palaeogeography, Palaeoclimatology, Palaeoecology, 248*(3–4), 291-312. doi:http://dx.doi.org/10.1016/j.palaeo.2006.12.008

Foden, J., Song, S. H., Turner, S., Elburg, M., Smith, P. B., Van der Steldt, B., & Van Penglis, D. (2002). Geochemical evolution of lithospheric mantle beneath S.E. South Australia. *Chemical Geology, 182*(2-4), 663-695.

Grey, K., Hocking, R. M., Stevens, M. K., Bagas, L., Carlsen, G., Irimies, F., Pirajno, F., Haines, P. W., & Apak, S. N. (2005). Lithostratigraphic nomenclature of the Officer Basin and correlative parts of the Paterson Orogen, Western Australia. *Western Australia Geological Survey Report*(93), 1-89.

Haines, P. W., & Allen, H. J. (2017). Geological reconnaissance of the southern Murraba Basin, Western Australia. *Geological Survey of Western Australia Record* (2017/4), 1-38.

Haines, P. W., Hocking, R. M., Grey, K., & Stevens, M. K. (2008). Vines 1 revisited: are older Neoproterozoic glacial deposits preserved in Western Australia? *Australian Journal of Earth Sciences, 55*(3), 397-406. doi:10.1080/08120090701769506

Haines, P. W., Mory, A. J., Stevens, M. K., & R, G. K. A. (2004). GSWA Lancer 1 well completion report (basic data), Officer and Gunbarrel Basins, Western Australia. *Geological Survey of Western Australia Record*(2004/10), 1-39.

Halverson, G. P., Hoffman, P. F., Schrag, D. P., Maloof, A. C., & Rice, A. H. N. (2005). Toward a Neoproterozoic composite carbon-isotope record. *Geological Society of America Bulletin, 117*(9-10), 1181-1207.

Hart, S. R. (1984). A large-scale isotope anomaly in the Southern Hemisphere mantle. *Nature, 309*(5971), 753-757.

Hill, A. C., Haines, P. W., & Grey, K. (2011). Chapter 67 Neoproterozoic glacial deposits of central Australia. *Geological Society, London, Memoirs, 36*(1), 677-691.

Hill, A. C., & Walter, M. R. (2000). Mid-Neoproterozoic (~830–750 Ma) isotope stratigraphy of Australia and global correlation. *Precambrian Research, 100*(1–3), 181-211. doi:http://dx.doi.org/10.1016/S0301-9268(99)00074-1

Hoffman, P. F., Kaufman, A. J., Halverson, G. P., & Schrag, D. P. (1998). A Neoproterozoic Snowball Earth. *Science, 281*(5381), 1342-1346.

Huang, Q., Kamenetsky, V. S., McPhie, J., Ehrig, K., Meffre, S., Maas, R., Thompson, J., Kamenetsky, M., Chambefort, I., Apukhtina, O., & Hu, Y. (2015). Neoproterozoic (ca. 820–830 Ma) mafic dykes at Olympic Dam, South Australia: Links with the Gairdner Large Igneous Province. *Precambrian Research, 271*, 160-172. doi:http://dx.doi.org/10.1016/j.precamres.2015.10.001

Ivanic, T. J., Nebel, O., Jourdan, F., Faure, K., Kirkland, C. L., & Belousova, E. A. (2015). Heterogeneously hydrated mantle beneath the late Archean Yilgarn Craton. *Lithos, 238*, 76-85. doi:http://dx.doi.org/10.1016/j.lithos.2015.09.020

Jourdan, F., Hodges, K., Sell, B., Schaltegger, U., Wingate, M. T. D., Evins, L. Z., Söderlund, U., Haines, P. W., Phillips, D., & Blenkinsop, T. (2014). High-precision dating of the Kalkarindji large igneous province, Australia, and synchrony with the Early–Middle Cambrian (Stage 4–5) extinction. *Geology, 42*(6), 543-546.

Kelley, S. (2002). Excess argon in K–Ar and Ar–Ar geochronology. *Chemical Geology, 188*(1–2), 1-22. doi:https://doi.org/10.1016/S0009-2541(02)00064-5

Kendall, B., Creaser, R. A., & Selby, D. (2006). Re-Os geochronology of postglacial black shales in Australia: Constraints on the timing of "Sturtian" glaciation. *Geology, 34*(9), 729-732.

Koppers, A. A. P. (2002). ArArCALC—software for 40Ar/39Ar age calculations. *Computers & Geosciences, 28*(5), 605-619. doi:https://doi.org/10.1016/S0098-3004(01)00095-4

Li, X.-H., Li, Z.-X., Wingate, M. T. D., Chung, S.-L., Liu, Y., Lin, G.-C., & Li, W.-X. (2006). Geochemistry of the 755 Ma Mundine Well dyke swarm, northwestern Australia: Part of a Neoproterozoic mantle superplume beneath Rodinia? *Precambrian Research, 146*(1–2), 1-15. doi:http://dx.doi.org/10.1016/j.precamres.2005.12.007

Macdonald, F. A., Schmitz, M. D., Crowley, J. L., Roots, C. F., Jones, D. S., Maloof, A. C., Strauss, J. V., Cohen, P. A., Johnston, D. T., & Schrag, D. P. (2010). Calibrating the Cryogenian. *Science, 327*(5970), 1241-1243.

Mark, D. F., Stuart, F. M., & de Podesta, M. (2011). New high-precision measurements of the isotopic composition of atmospheric argon. *Geochimica et Cosmochimica Acta, 75*(23), 7494-7501. doi:http://dx.doi.org/10.1016/j.gca.2011.09.042

McDonough, W. F., & Sun, S. s. (1995). The composition of the Earth. *Chemical Geology, 120*(3-4), 223-253.

Morton, J. G. G. (1997). Chapter 6: Lithostratigraphy and environments of deposition. In J. G. G. Morton & J. F. Drexel (Eds.), *The petroleum geology of South Australia. Volume 3: Officer Basin* (pp. 47-86): South Australia Department of Mines and Energy Resources, Report Book 97/19.

Pfander, J. A., Munker, C., Stracke, A., & Mezger, K. (2007). Nb/Ta and Zr/Hf in ocean island basalts -- Implications for crust-mantle differentiation and the fate of Niobium. *Earth and Planetary Science Letters, 254*(1-2), 158-172.

Pirajno, F., Haines, P. W., & Hocking, R. M. (2006). Keene Basalt, northwest Officer Basin, Western Australia: tectonostratigraphic setting and implications for possible submarine mineralisation. *Australian Journal of Earth Sciences, 53*(6), 1013-1022. doi:10.1080/08120090600883374

Pisarevsky, S. A., Wingate, M. T. D., Li, Z.-X., Wang, X.-C., Tohver, E., & Kirkland, C. L. (2014). Age and paleomagnetism of the 1210 Ma Gnowangerup–Fraser dyke swarm, Western Australia, and implications for late Mesoproterozoic paleogeography. *Precambrian Research, 246*(0), 1-15. doi:http://dx.doi.org/10.1016/j.precamres.2014.02.011

Pisarevsky, S. A., Wingate, M. T. D., Powell, C. M., Johnson, S., & Evans, D. A. D. (2003). Models of Rodinia assembly and fragmentation. *Geological Society, London, Special Publications, 206*(1), 35-55.

Pisarevsky, S. A., Wingate, M. T. D., Stevens, M. K., & Haines, P. W. (2007). Palaeomagnetic results from the Lancer 1 stratigraphic drillhole, Officer Basin, Western Australia, and implications for Rodinia reconstructions. *Australian Journal of Earth Sciences, 54*(4), 561-572. doi:10.1080/08120090701188962

Prave, A. R., Condon, D. J., Hoffmann, K. H., Tapster, S., & Fallick, A. E. (2016). Duration and nature of the end-Cryogenian (Marinoan) glaciation. *Geology, 44*(8), 631-634.

Preiss, W. V. (2000). The Adelaide Geosyncline of South Australia and its significance in Neoproterozoic continental reconstruction. *Precambrian Research, 100*(1–3), 21-63. doi:http://dx.doi.org/10.1016/S0301-9268(99)00068-6

Preiss, W. V., Drexel, J. F., & Reid, A. J. (2009). Definition and age of the Kooringa Member of the Skillogalee Dolomite: host for Neoproterozoic (c. 790 Ma) porphyry-related copper mineralisation at Burra. *MESA Journal, 55*, 19-33.

Rasmussen, B., & Fletcher, I. R. (2004). Zirconolite: A new U-Pb chronometer for mafic igneous rocks. *Geology, 32*(9), 785-788.

Renne, P. R., Balco, G., Ludwig, K. R., Mundil, R., & Min, K. (2011). Response to the comment by W.H. Schwarz et al. on "Joint determination of 40K decay constants and 40Ar∗/40K for the Fish Canyon sanidine standard, and improved accuracy for 40Ar/39Ar geochronology" by P.R. Renne et al. (2010). *Geochimica et Cosmochimica Acta*, *75*(17), 5097-5100. doi:https://doi.org/10.1016/j.gca.2011.06.021

Renne, P. R., Deino, A. L., Hilgen, F. J., Kuiper, K. F., Mark, D. F., Mitchell, W. S., Morgan, L. E., Mundil, R., & Smit, J. (2013). Time Scales of Critical Events Around the Cretaceous-Paleogene Boundary. *Science, 339*(6120), 684.

Rooney, A. D., Strauss, J. V., Brandon, A. D., & Macdonald, F. A. (2015). A Cryogenian chronology: Two long-lasting synchronous Neoproterozoic glaciations. *Geology*, *43*(5), 459-462.

Sun, S. s., & McDonough, W. F. (1989). Chemical and isotopic systematics of oceanic basalts: implications for mantle composition and processes. In A. D. Saunders & M. J. Norry (Eds.), *Magmatism in the Ocean Basins* (Vol. 42, pp. 313-345).

Swanson-Hysell, N. L., Maloof, A. C., Condon, D. J., Jenkin, G. R. T., Alene, M., Tremblay, M. M., Tesema, T., Rooney, A. D., & Haileab, B. (2015). Stratigraphy and geochronology of the Tambien Group, Ethiopia: Evidence for globally synchronous carbon isotope change in the Neoproterozoic. *Geology*, *43*(4), 323-326.

Swanson-Hysell, N. L., Maloof, A. C., Kirschvink, J. L., Evans, D. A. D., Halverson, G. P., & Hurtgen, M. T. (2012). Constraints on Neoproterozoic paleogeography and Paleozoic orogenesis from paleomagnetic records of the Bitter Springs Formation, Amadeus Basin, central Australia. *American Journal of Science*, *312*(8), 817-884.

Swanson-Hysell, N. L., Rose, C. V., Calmet, C. C., Halverson, G. P., Hurtgen, M. T., & Maloof, A. C. (2010). Cryogenian Glaciation and the Onset of Carbon-Isotope Decoupling. *Science*, *328*(5978), 608-611.

Torsvik, T. H., Ashwal, L. D., Tucker, R. D., & Eide, E. A. (2001). Neoproterozoic geochronology and palaeogeography of the Seychelles microcontinent: the India link. *Precambrian Research*, *110*(1–4), 47-59. doi:https://doi.org/10.1016/S0301-9268(01)00180-2

Verati, C., & Jourdan, F. (2014). Modelling effect of sericitization of plagioclase on the $^{40}$K/$^{40}$Ar and $^{40}$Ar/$^{39}$Ar chronometers: implication for dating basaltic rocks and mineral deposits. *Geological Society, London, Special Publications, 378*(1), 155.

Walter, M. R., Veevers, J. J., Calver, C. R., Gorjan, P., & Hill, A. C. (2000). Dating the 840–544 Ma Neoproterozoic interval by isotopes of strontium, carbon, and sulfur in seawater, and some interpretative models. *Precambrian Research*, *100*(1–3), 371-433. doi:http://dx.doi.org/10.1016/S0301-9268(99)00082-0

Walter, M. R., Veevers, J. J., Calver, C. R., & Grey, K. (1995). Neoproterozoic stratigraphy of the Centralian Superbasin, Australia. *Precambrian Research, 73*(1–4), 173-195. doi:http://dx.doi.org/10.1016/0301-9268(94)00077-5

Wang, X.-C., Li, X.-H., Li, Z.-X., Liu, Y., & Yang, Y.-H. (2010). The Willouran basic province of South Australia: Its relation to the Guibei large igneous province in South China and the breakup of Rodinia. *Lithos, 119*(3–4), 569-584. doi:https://doi.org/10.1016/j.lithos.2010.08.011

Ware, B., & Jourdan, F. (2018). $^{40}Ar/^{39}Ar$ geochronology of terrestrial pyroxene. *Geochimica et Cosmochimica Acta, 230*, 112-136. doi:https://doi.org/10.1016/j.gca.2018.04.002

Wingate, M. T. D. (2017). Mafic dyke swarms and large igneous provinces in Western Australia get a digital makeover. *GSWA 2017 extended abstracts*(Record 2017/2), 4-8.

Wingate, M. T. D., Campbell, I. H., Compston, W., & Gibson, G. M. (1998). Ion microprobe U–Pb ages for Neoproterozoic basaltic magmatism in south-central Australia and implications for the breakup of Rodinia. *Precambrian Research, 87*(3–4), 135-159. doi:http://dx.doi.org/10.1016/S0301-9268(97)00072-7

Wingate, M. T. D., & Giddings, J. W. (2000). Age and palaeomagnetism of the Mundine Well dyke swarm, Western Australia: implications for an Australia–Laurentia connection at 755 Ma. *Precambrian Research*, *100*(1–3), 335-357. doi:http://dx.doi.org/10.1016/S0301-9268(99)00080-7

Zhao, J.-X., McCulloch, M. T., & Korsch, R. J. (1994). Characterisation of a plume-related ~ 800 Ma magmatic event and its implications for basin formation in central-southern Australia. *Earth and Planetary Science Letters, 121*(3–4), 349-367. doi:http://dx.doi.org/10.1016/0012-821X(94)90077-9

Zindler, A., & Hart, S. (1986). Chemical geodynamics. *Annual review of Earth and planetary sciences. Vol. 14, Published by Annual Reviews Inc., Editors Wetherill G.W. and et al.*, 493-571.